Study of the Transverse Coherence at the TTF Free Electron Laser

R. Ischebeck[a*], J. Feldhaus[b], Ch. Gerth[b], E. Saldin[b], P. Schmüser[c], E. Schneidmiller[b], B. Steeg[b], K. Tiedtke[b], M. Tonutti[a], R. Treusch[b], M. Yurkov[d]

[a]Rheinisch-Westfälische Technische Hochschule Aachen, III. Physikalisches Institut, Sommerfeldstraße 14, 52056 Aachen, Germany

[b]Deutsches Elektronen-Synchrotron DESY, Notkestraße 85, D-22603 Hamburg, Germany

[c]Universität Hamburg und DESY, Notkestraße 85, D-22603 Hamburg, Germany

[d]Joint Institute for Nuclear Resaerch, Dubna, 141980 Moscow Region, Russia

Double slits with different separations, crossed slits and circular apertures have been used to study the transverse coherence of the VUV light of the SASE Free Electron Laser at the TESLA Test facility at DESY. The resulting diffraction patterns are converted to visible light by a Ce:YAG crystal and imaged by a high resolution CCD camera. The visibility of the diffraction patterns indicates a high degree of transverse coherence. Measurements have been taken at various operating modes and wavelengths of the FEL. A numeric FEL simulation code (FAST) has been used to calculate the wavefronts of the light at the exit of the undulator. By propagating the wavefronts through the optical setup, the diffraction at the double slits is computed with the code GLAD. Good agreement with the measurements is found.

1. Transverse Coherence

Transverse coherence is one of the key features of a free electron laser. The particles in each microbunch oscillate synchronously; this is the reason for the enormous brilliance growth as compared to a conventional undulator light source. At the same time, the synchronized motion creates a radiation with a high degree of transverse coherence. The coherence increases as the FEL reaches saturation.

A light pulse can be characterized by its longitudinal and transverse coherence properties[2]. The transverse coherence has been investigated with the classical Young double slit experiment. The FEL beam propagates in free space behind the undulator, and the transverse coherence length increases together with the beam width during propagation of the light pulse. Hence the position must be specified at which the coherence length is determined. In the present expertiment, we choose the position of the double slits, 11.84 m downstream of the undulator exit. The complete setup is enclosed in the ultra high vacuum environment of the accelerator to avoid absorption of the VUV light.

2. TTF Accelerator and Free Electron Laser

The linear accelerator at the TESLA Test Facility TTF [1], [2] is equipped with 17 nine-cell superconducting cavities and serves both as a test accelerator for the superconducting linear electron-positron collider TESLA and as a drive linac for a VUV free electron laser which is based on the Self Amplified Spontaneous Emission (SASE) principle. The maximum electron energy is 260 MeV, the maximum bunch charge 5 nC. For the present measurements, photon wavelengths between of 80 and 120 nm have been used. The total pulse energy can reach 10 μJ.

*Corresponding author. E-mail: Rasmus.Ischebeck@desy.de

[2]These are also called temporal and spatial coherence.

3. Photon Diagnostics

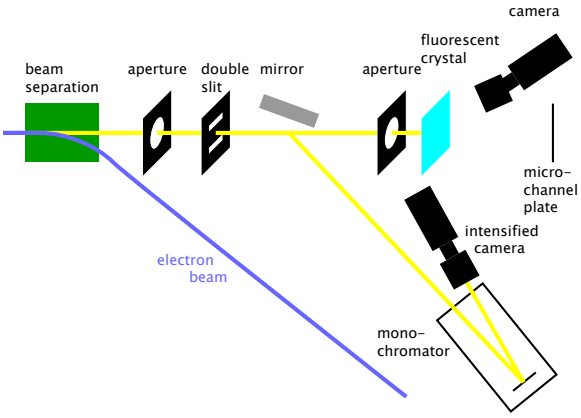

Figure 1. *Experimental setup for the SASE FEL photon diagnostics at the TTFL. For details, see [3].*

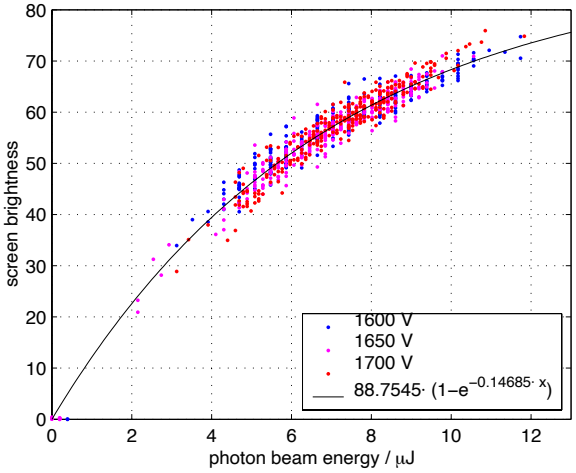

Figure 2. *Correlation of the Ce:YAG crystal brightness with the calibrated signal of the multi channel plate detector. The MCP has been operated at three different operating voltages; the results have been scaled according to a previous calibration [4]. The black line gives the fitted curve.*

Various devices are installed to analyze the properties of the FEL light. Figure 1 shows an overview of the experimental setup. A grating spectrometer [3], equipped with an intensified CCD camera, is used to measure the spectral distribution. The intensity is monitored over a wide range with a calibrated micro-channel plate (MCP) [4], detecting the light which is scattered on a thin gold-plated tungsten wire. A fluorescent Ce:YAG crystal (cerium activated yttrium aluminum garnet $Y_3Al_5O_{12} : Ce$) can be inserted to observe the spatial distribution of the FEL light as well as interference patterns. Ce:YAG is a fast scintillator (decay time constant 80 ns) with excellent mechanical properties. A crystal made of lead tungstenate ($PbWO_4$) is also available. However, in light yield it is much inferior to the Ce:YAG screen.

The light output of the Ce:YAG crystal is a non-linear function of the incident photon pulse energy, see Fig. 2. The MCP detector has been used to determine the light pulse energy.

The crystal is observed by a CCD camera, having 1280×1024 pixels with a size of $(6\,\mu\text{m})^2$. A Peltier element cools the CCD in order to reduce noise and to make use of the full range of the 12 bit ADC. The camera is controlled and read out by a fiber optical link. The CCD chip employs the interline transfer technique to achieve exposure times below one microsecond and the lens-on-chip technique to increase the sensitivity. The CCD signal is digitized in the camera itself. In comparison with conventional video technology, where an analogue signal is transmitted to a frame grabber outside of the accelerator area, the digital readout reduces crosstalk to a minimum and permits a precise timing between the charge transfer in the CCD and the digitization of the ADC.

The space behind the Ce:YAG screen is occupied by an MCP detector. Therefore, the CCD camera is mounted at an angle of approximately 35° with respect to the normal of the screen. A shift-tilt lens (Nikon 85mm f/2.8D) is used to achieve good focusing over the entire crystal area. Different apertures can be moved into the beam at a position 3.1 m in front of the screen and

11.84 m behind the undulator exit. Circular apertures and double slit arrangements with different separations are mounted on two actuators. They can be moved to an arbitrary position with stepper motors. The slits are 2 mm long and 100 μm respectively 200 μm wide.

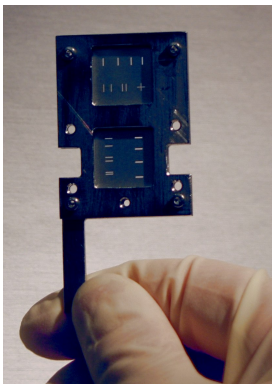

Figure 3. *The double slits, cut in stainless steel foil.*

Due to the high absorption of 100 nm radiation by almost any material, it is not possible to extract the radiation from the accelerator beam tube through an optical window. Therefore, the entire setup is incorporated into the accelerator vacuum system. As a consequence, the slit arrangement and the distance between slits and screen cannot be varied easily. The CCD camera is protected against radiation damage by a 20 cm thick lead shielding.

4. Image Processing

The image Φ recorded by the CCD is the convolution of the actual diffraction pattern Ψ with the point spread function P of the lens:

$$\Phi(x,y) = \int_{-\infty}^{\infty}\int_{-\infty}^{\infty} P(x-u, y-v)\cdot\Psi(u,v)\mathrm{d}u\ \mathrm{d}v$$

or, if we use discrete distributions

$$\Phi_{i,k} = \sum_{m,n} P_{i-m,k-n}\cdot\Psi_{m,n} \qquad (1)$$

The finite resolution smears out details in the images and reduces the apparent visibility of the diffraction patterns.

The system of equations (1) can in principle be solved for Ψ by matrix inversion if the point spread function P is accurately known. However, noise in the measured image distribution has a strong impact on the solution and will inevitably lead to negative values for Ψ. More appropriate are methods based on the maximum likelihood principle, imposing additional constraints on the smoothness and non-negativity of the reconstructed distribution. Originally developed by Lucy [5] and Richardson, such methods are widely used to correct for lens errors.

The point spread function may depend on the position in the image. Lens errors, for example, become more important in the outer part of the observed field. In our case, the tilt of the lens was not completely sufficient to correct for the inclination of the Ce:YAG crystal. A deconvolution with a spatially varying point spread function is numerically elaborate since it cannot be done in Fourier space [6].

The point spread function (PSF) of our setup has been measured in the center of the image with the lens focused onto an aperture with 1 μm diameter, illuminated from the back side by incoherent light. The width of the PSF increases as one moves away from the center. The narrow PSF has been used in the data analysis in order to avoid that an image is reconstructed with a higher contrast than is present in the real diffraction pattern (Fig. 4). The nonlinear response of the Ce:YAG has been corrected for using the fit curve in (Fig. 2).

It should be noted that the Ce:YAG crystal has another effect on the measured contrast of the interference pattern. The visible photons produced by fluorescence are emitted with an isotropic distribution. Only part of them enter the camera directly while many others are internally reflected at the surface of the crystal and emerge at the edges. On their path some are scattered inside the crystal and generate thereby an overall light background that reduces the modulation visibility of the diffraction pattern. The effect is under study but the data presented here are not yet cor-

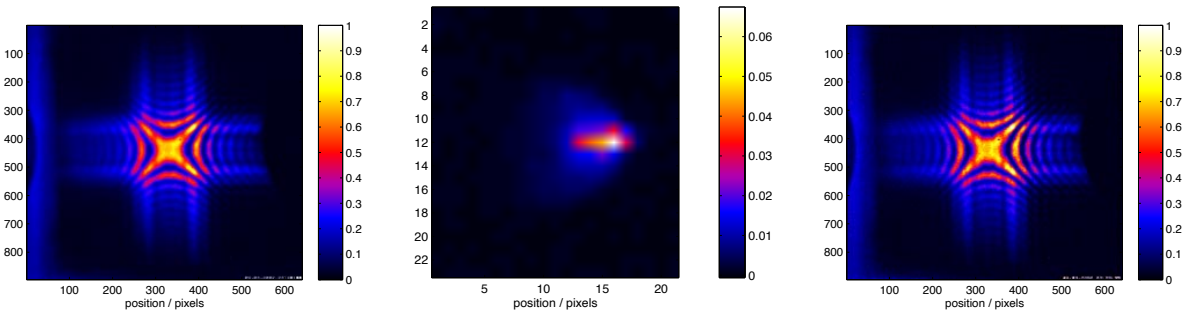

Figure 4. Left: *Raw image, averaged from 100 pictures; units: ADC counts.* Middle: *Point spread function of the tilted lens, measured under the same conditions as in the FEL.* Right: *The image has been deconvoluted with the camera resolution (10 iterations of the Lucy-Richardson algorithm [5]).*

rected for this background.

5. Image Analysis

To extract a quantitative measure for the transverse coherence from the images, the following analysis routine is applied. A slice perpendicular to the slits is selected and projected onto an axis along the slit direction. The resulting curve is smoothed with a fifth order lowpass Butterworth filter. One defines the *visibility* as the modulation depth of the intensity:

$$\mathcal{V} = \frac{I_{max} - I_{min}}{I_{max} + I_{min}}$$

and is computed for each interference fringe. For a perfectly coherent beam, we expect $\mathcal{V} = 1$ in the center of the pattern. Due to near field effects, the visibility drops to zero towards the sides (see section 6). Its peak value can be taken as a measure for the transverse coherence of the FEL beam at the given slit separation. The dependence of $\mathcal{V}$ on the slit separation is shown in Fig. 6. The measured [7] and simulated [8] beam profiles are shown for comparison.

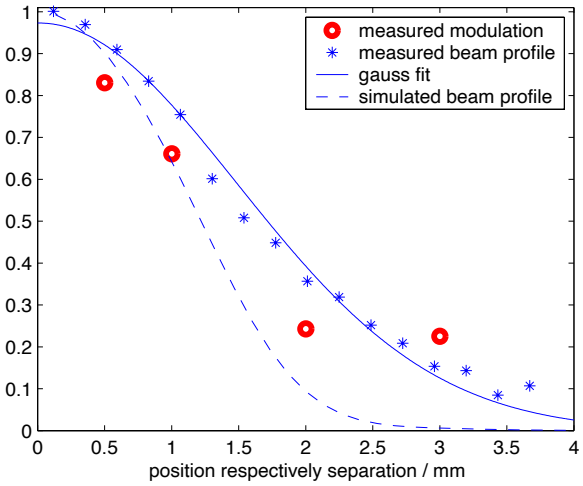

Figure 6. *Central modulation as a function of slit separation. For comparison, the beam profile (measured with the MCP detector) is also shown.*

6. Simulations

At a distance of 3.1 m behind the double slit one has not yet arrived in a region where far field diffraction theory (Fraunhofer diffraction) is applicable. Therefore, the diffraction effects are simulated with the program GLAD [9] which takes into account near field effects by solving

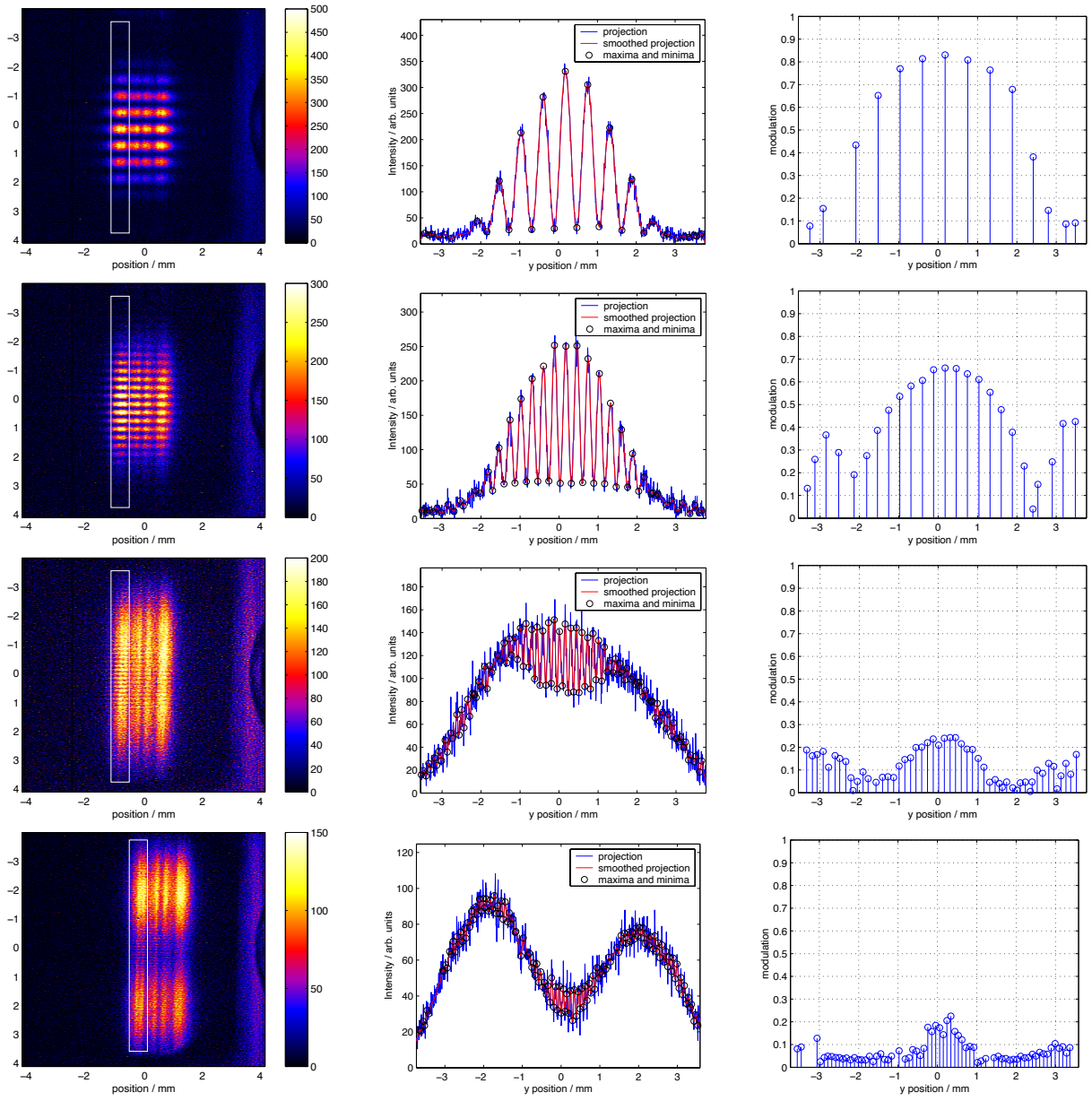

Figure 5. *Diffraction pattern for horizontal double slits with 0.5, 1, 2 and 3 mm separation.* Left: *Camera images*, middle: *Projection of the selected region*, right: *Visibility of the diffraction fringes.* First row: *0.5 mm*, second row: *1 mm*, third row: *2 mm and* fourth row: *3 mm slit separation. The visibility is highest in the middle of the field (although the envelope of the pattern has a minimum for the slits separated by 3 mm). The data are preliminary since a correction for background light in the Ce-YAG screen has not yet been applied.*

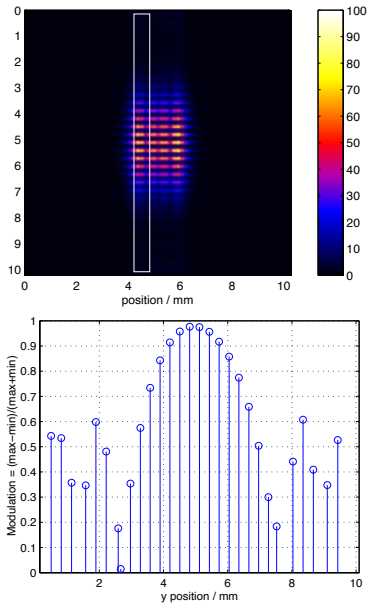

Figure 7. *Simulated diffraction pattern for the double slits with 1 mm separation.* Top: *Intensity distribution.* Bottom: *Visibility of the diffraction fringes.*

the Maxwell equations on a discrete grid that is propagated through space. The simulations are done on a grid of 2048 × 2048 points with a separation of 5 μm. The output wave front of the three-dimensional FEL simulation code FAST [8] is propagated from the end of the undulator through the slits up to the Ce:YAG screen. Fifty slices, equally spaced over the bunch, are propagated individually and their intensity at the screen is added incoherently. The resulting visibility (Fig. 7) is only slightly lower than unity.

7. Conclusion and Outlook

We have installed and successfully operated a double slit experiment at the 100 nm FEL at DESY. The observed diffraction pattern is quite similar to a numerical simulation in the near-field regime. The measured modulation depth exceeds a value 0.8 at 0.5 mm slit separation and goes down with increasing separation. It sould be noted though that the true modulation depth will be larger since a correction for the background light in the Ce:YAG screen has not yet been applied. From a statistical analysis of the FEL data almost full transverse coherence can be derived [10].

Beyond the saturation point of the FEL, the number of transverse modes grows, leading to a decrease of the transverse coherence. The TTF FEL can be virtually shortened by kicking the beam away from the undulator axis at various positions along the undulator. Thereby, it was possible to record diffraction patterns with different effective undulator lengths. The analysis of these data is underway.

REFERENCES

1. The Conceptual Design Report for the TESLA Test Facility, http://tesla.desy.de/TTF_Report/CDR/TTFcdrTab.html
2. P. Castro, Performance of the TESLA Test Facility Linac EPAC 2002
3. Ch. Gerth et al., Nucl. Instr. and Methods **A 475** (2001) 481
4. B. Faatz et al., TESLA-FEL 2001-09, 62 – 67
5. L. B. Lucy, The Atronomical Journal Vol. 79, Nb. 6, (1974) 745.
6. A.F. Boden, D.C. Redding, R.J. Hanisch, and J. Mo J. Opt. Soc. of America A, V 13 No 7 (1996) 1537 – 1545.
7. V. Ayvazian et al., Phys. Rev. Lett. **88** (2002) 10482.
8. E. L. Saldin, E. A. Schneidmiller, M. V. Yurkov, Nucl. Instrum. and Methods **A 429**, 233 (1999)
9. Applied Optics Research, http://www.aor.com
10. E.L. Saldin, E.A. Schneidmiller, M.V. Yurkov, these Proceedings.